

RADIATION EFFECTS ON SUPERCONDUCTING MAGNETS*

H. Brechna
Stanford Linear Accelerator Center
Stanford University, Stanford, California

I. INTRODUCTION

When subjected to nuclear radiation, superconducting materials, normal metals, structural materials, insulation and the cooling media - in short, the superconducting magnet system - exhibit changes where physical and mechanical properties are altered, modified or degraded. The changes depend on the type of particles, the intensity, spread and distribution of the beam, the irradiation pattern, and the type of material being irradiated.

In order to study radiation effects on a superconducting magnet in a systematic way, the following areas where obvious modifications are encountered are summarized.

- 1) Physical and metallurgical properties of superconducting type II materials are changed.
- 2) Mechanical, electrical and thermal properties of normal shunt materials, thermoelectrically bonded to the superconductor, are altered.
- 3) Structural and coil supporting materials are affected.
- 4) Organic insulation used between turns and between coils and ground is degraded.
- 5) The coolant, such as helium, is contaminated, and isotopes are produced.
- 6) Coolant is evaporated at an accelerated rate, and mass transfer between liquid and gas is enhanced.

The mechanisms responsible for large transport currents in type II superconductors are attributed mainly to cold-working and introduction of defect structures, and through enhancement of the pinning force. Controlled introduction of impurities results in enhancement of current density. Precipitated impurities affect the current density in a reproducible manner.¹

The primary effect of nuclear radiation is the introduction in the lattice structure of simple defects which affect the critical supercurrent, the upper critical field and the critical temperature.

When irradiated at a temperature below transition value, low-current, high-field type II superconductors generally show an enhancement in their critical current density J_c ; high-current-density superconductors exhibit either no change or a reduction in their current-carrying capacity - e.g., Nb_3Sn shows generally an improvement in J_c when irradiated, while irradiated $NbTi$ exhibits a reduction in current-carrying capacity when irradiated at $T < T_c$.

*Work supported by the U.S. Atomic Energy Commission.

1. H.T. Coffey et al., Phys. Rev. 155, 355 (1967).

Normal shunt materials (Cu, Al, Ag) become brittle. Their electrical resistivity is increased, thermal conductivity reduced.

Organic materials used to insulate conductors and coils show embrittlement and become crush sensitive. When insulation properties are degraded, interturn and inter-layer short circuits are produced, affecting over-all magnet charging time. If the short circuits are localized in one area, the magnet energy will be dissipated in case of a quench into this area, causing extensive damage to the magnet.

Liquid helium boil-off is generally enhanced. Even if the additional helium evaporation is moderate, in case of localized irradiation, isotopes, such as tritium, hydrogen, etc., are produced which, in frozen condition, may restrict coolant passages and affect operational reliability.

The study presented in this paper is at a very preliminary stage and is by no means complete. Considerably more work is needed to predict the lifetime of a magnet, operating in a radiation environment. However, the data presented should shed some light on this complex subject in order to determine the magnet degradation and predict operational stability.

II. INDUCED RADIOACTIVITY

Induced activity exists in almost any accelerator. Radiation encountered includes fast and thermal neutrons, gammas, electrons and positrons, and protons. In electron accelerators, the electromagnetic shower develops in a short distance. Activation due to neutron capture reaction is less severe than in proton machines of equal power because of cross section for nuclear interaction. However, ionizing radiation fields are much larger.²

"Meson factories" produce a localized source of fast neutrons. High energy proton machines produce intense fast neutrons. But the shower is spread over large volumes and thus is less damaging.

In designing specific beam transport and septum magnets, dipole coils, etc., one important problem is the knowledge of the beam pattern throughout the system. In areas where the beam is deliberately absorbed, intense activation will exist. Penetration, scattering and "tails" of energy spectra are encountered around slits and collimators, as well as around targets. Activation due to beam absorbers exists in other locations of the system, endangering the long-term reliability of equipment and magnets.

Exact prediction of beam losses is difficult, but activity measurements in the early life of accelerators may reveal areas of high activation, where, if possible, appropriate measurements may be taken. Long-term continuous radiation measurements will yield undoubtedly the average integrated dose rates, which in turn are important to predict lifetime of equipment. Several systems of dosimeters are currently being utilized with good success in "danger" areas.^{3,4}

To a certain extent, quantitative data on radiation properties of ferrous and non-ferrous materials, insulations, and superconductive type II materials are available at cryogenic temperatures. Although sketchy and not complete, they give a first-order

2. R.E. Taylor, IEEE Trans. Nucl. Sci. NS-12, No. 3, 846 (1965).

3. R. Sheldon, Rutherford High Energy Laboratory (1966).

4. M.H. Van de Voorde, Report CERN 67-14 (1967).

estimation of the average life expectancy of magnets. More information on material properties when irradiated at 2-10°K is urgently required, when superconducting magnets are introduced in vital areas of high-energy accelerators.

In order to present some quantitative data on beam losses, one may simulate the "deliberate" beam absorption by means of collimators, slits, or by accidental beam missteering in linear machines or beam switchyards by means of "thick target" studies, where the target length and radial extension exceed several radiation lengths. A charged particle, traversing the magnet, undergoes a large number of collisions, most of which produce small angular deflections. The particles lose energy by collision (pair production) and radiation. Exact estimates of the average dose rate are difficult and we use simplified models. Careful radiation mapping will give a good estimate of dose rates, specifically incident to beam entry direction and perpendicular to it.

Activation due to partial beam absorption by means of thin targets is also of importance.

In the following, we treat each case in more detail.

1. Thick Targets

Any obstacle in the path of the beam having dimensions of several radiation lengths in axial X_0 (beam direction) and radial X_m directions (perpendicular to beam direction), being able to absorb most of the incident beam, can be considered as a thick target. Three types of particles are observed in conjunction with them:

a. Gammas. Measurements by DeStaebler et al.⁵ indicate that induced dose rates for gammas are independent of the beam energy as first approximation (Fig. 1) and of the target material. For a cylindrical target having a length of 17 X_0 and a radius of 3.6 X_m , Jenkins⁶ measured for $\theta = 0$ a dose rate of

$$2 \times 10^5 \frac{\text{rad}}{\text{h}} \cdot \frac{\text{m}^2}{\text{kW}}$$

As seen from Fig. 2, the energy spread over 4π sr is fairly isotropic. If we assume that 1% of the total energy escapes radially (Fig. 1), an average dose of

$$\bar{D} = 10^3 \frac{\text{rad}}{\text{h}} \cdot \frac{\text{m}^2}{\text{kW}}$$

can be calculated. To give an example, we assume that a coil is located 5 m from the thick target, where a beam power of 10 kW is absorbed. Generally the magnet dimensions are large enough that we can assume that all scattered particles may collide with the coil surface perpendicular to the incident beam direction.

A radiation dose rate D (rad/h) is equivalent to

$$\frac{D}{3.6 \times 10^8} \frac{\text{W}}{\text{g}}$$

5. H. DeStaebler et al., The Stanford Two-Mile Accelerator (W.A. Benjamin Publishing Co., 1968), Chap. 26, p. 1029.

6. T.M. Jenkins, Report SLAC-PUB-432, to be published in Health Physics (1968).

The beam power induced by the scattered beam dissipated in a volume V of the magnet is given by

$$P_d = \frac{1}{3.6 \times 10^8} \int_V D \delta(V) dV \quad (W) \quad (1)$$

If the total dose rate D is absorbed by the coil and we estimate for the density δ of the coil an average value of 5 g/cm³, the power dissipated is

$$P_d = 1.388 \times 10^{-8} \overline{DV} \quad .$$

This additional power must be absorbed by the coolant. The integrated dose rate for this particular case can be calculated from:

$$d = 0.4 \times 10^3 \text{ rad/h} \quad .$$

b. Fast neutrons. Except in the forward direction, where production of muons becomes significant, neutrons with energies of 200-500 MeV dominate in high-energy accelerators. Higher energy neutrons are scarce because there are very few high-energy photons. Neutrons with lower energies have short attenuation distances and are more readily absorbed.

Neutron fluxes in the giant resonance region were measured at SLAC,⁶ indicating that it is isotropic within a factor of 2.5 or better, if the effect of back-scatter is added. At an angle of 90° with respect to the incident beam, a neutron flux of 1.25×10^{12} n/sec/kW could be measured. Assuming the flux distribution is isotropic, the flux at one-meter distance is expressed by

$$\phi = \frac{1.25 \times 10^{12}}{4\pi \times 10^4} \frac{n}{\text{sec} \cdot \text{kW}} \quad (2)$$

The neutron dose for 1 kW beam power at 1 m distance at 2-3 MeV peak neutron energies is given by:

$$\begin{aligned} \overline{D}_N &= \frac{1.25 \times 10^{12}}{4\pi \times 10^4} \times 6 \times 10^{-9} \times 3.6 \times 10^3 \\ &\cong 2.5 \times 10^2 \frac{\text{rad}}{\text{h}} \cdot \frac{\text{m}^2}{\text{kW}} \quad . \end{aligned}$$

(We use the conversion factor 6×10^{-9} rad/n/cm².)

The integrated dose rate for $r = 5$ m and $P = 10$ kW gives the integrated dose rate of $d = 10^2$ rad/h.

c. Muons. Muons lose energy by ionization and thus a unique range is associated with each energy. However, muons penetrate thick shielding of several meters in depth without appreciable energy loss. For electron and proton machines, high-energy muons are peaked predominantly in the forward direction. Transverse shielding is of no consequence. However, muons are still scattered up to angles of $\pm 5^\circ - 8^\circ$ off the incident beam. Nelson⁷ has measured muon peak dose rates without shielding of about

7. W.R. Nelson, Report SLAC-PUB-481, to be published in Nucl. Instr. and Methods (1968).

$$D_{\mu} = 10^2 \frac{\text{rad}}{h} \cdot \frac{m^2}{\text{kW}}$$

2. Thin Targets

Multiple scattering was studied by Molière⁸ and recently by Marion and Zimmerman.⁹ To determine the fraction of scattered electrons due to an incident electron beam of energy E_0 passing through a thin target, data presented by Marion and Zimmerman and experimental results at SLAC⁶ are used.

The angular distribution of scattered particles, concentrated at a forward angle, is approximately Gaussian, of the form

$$f(X) = e^{-(X/X_W)^2}$$

where X_W is the value of X at the $1/e$ point. The differential angular distribution is a slowly varying function of the parameter B :

$$X_W^2 = 0.159 \frac{Z(Z+1)}{A} \cdot \frac{t}{(p\beta c)^2} \cdot B \quad (3)$$

where t = target thickness in (g/cm^2),
 Z = atomic number,
 A = atomic weight,
 $(p\beta c)^2$ = relativistic particle energy $\cong E_0$.

At values of X larger than for the $1/e$ point, the distribution falls more slowly due to wide-angle scattering contributions. The shape of the scattering distribution may be described by curves for various values of the parameter B . The differential distribution (function of X) must be integrated over all angles to find the fractions of electrons $G(X)$ that are scattered out of a cone of a given angle. This fraction is also a function of the parameter B .

For various target materials and thicknesses, Jenkins⁶ has published B values. In Fig. 3, the calculated B value for copper is given. If the location of the target to a point in space, where activation must be determined, is known, we may calculate for various values of the scattering angle θ the corresponding value $\theta = X \cdot X_W$ and obtain from Fig. 3 the fraction of the scattered beam at the specific point in space. As an example, we use a copper target with

$$\begin{aligned} t &= 0.1 \text{ radiation length} \\ &= 0.1 \times 13.1 = 1.31 \text{ g}/\text{cm}^2 \\ Z &= 29 \\ A &= 63.54 \\ B &\cong 10 \end{aligned}$$

We calculate from Eq. (3) $X_W \cong 5.35/E_0$ (with E_0 in MeV).

8. G. Molière, Z. Naturforsch. 2a, 133 (1947); 3a, 78 (1948).

9. J.B. Marion and B.A. Zimmerman, Nucl. Instr. and Methods 51, 93 (1967).

For $E = 10$ GeV, we calculate the radius r at which 0.1% of the energy scattered. From Fig. 3, for $B = 10$, we get $X = 9.7$ and thus

$$\theta = 9.7 \times \frac{5.35}{10 \times 10^3} \cong 5.2 \text{ mrad} .$$

To determine the activation in superconducting coils, located at a certain distance from the thin target, the coil surface perpendicular to the incident beam direction may be subdivided into sections where θ can be measured. With a given value of X_W , we calculate X and determine from Fig. 4 the fraction of the incident beam energy. To obtain the dissipated power due to radiation, one may use the method described for thick targets in Section II.1.

3. Maximum Expected Radiation Dose Inside Magnet Coils

For the buildup of showers inside coils, the variable collision loss is replaced by a constant collision loss ϵ_0 , called the "critical energy," which is the ionization loss per radiation length X_0 expressed in g/cm^2 .

We confine the calculation to particle energies large compared to the critical energy. If the incident energy E_0 is large, or:

$$E_0 \gg \frac{1}{\alpha} m_e \cdot c^2 Z^{-1/3} , \quad (4)$$

the shower may be described by "Approximation B," according to Rossi,¹⁰ where:

$$\frac{1}{\alpha} = \frac{\hbar c}{e^2} = 137 \quad \text{structure constant}$$

$$m_e = 9.105 \times 10^{-28} \text{ g} \quad \text{electron rest mass}$$

$$Z = 29 \quad \text{atomic number for Cu} .$$

We use as an example the electron beam energy at SLAC:

$$E_i = 20 \text{ GeV} ,$$

and get

$$E_i = 20 \times 10^9 \text{ eV} \gg 2.286 \times 10^7 \text{ eV} .$$

For copper the radiation length is $X_0 = 13.1 \text{ g}/\text{cm}^2$ and the critical energy

$$\epsilon_0 = 20.9 \times 10^6 \text{ eV} .$$

The average energy loss per particle per unit length (g/cm^2) is calculated from:

$$-\frac{dE}{dX} = \frac{\epsilon_0}{X_0} \quad (5)$$

$$\cong 1.6 \text{ MeV/g} \quad (\text{for copper}) .$$

10. B. Rossi, High Energy Particles (Prentice-Hall, New York, 1953).

The length where the shower maximum is reached is calculated according to Approximation B from:

$$\left(\frac{X}{X_0} \right)_{\max} = 1.01 \left[\ln \frac{E_0}{\epsilon_0} - 1 \right] . \quad (6)$$

At the shower peak, the number of electrons is given by:

$$n_{\max} = n_0 \cdot \frac{0.31}{\left[\ln \frac{E_0}{\epsilon_0} - 0.37 \right]^{\frac{1}{2}}} \cdot \frac{E_0}{\epsilon_0} , \quad (7)$$

where n_0 is the incident number of electrons. Combining Eq. (5) and Eq. (7), we get:

$$-\frac{n_{\max}}{n_0} \frac{dE}{dX} = \frac{0.31}{\left[\ln \frac{E_0}{\epsilon_0} - 0.37 \right]^{\frac{1}{2}}} \cdot \frac{E_0}{X_0} . \quad (8)$$

Equation (8), multiplied by the beam current density in A/cm^2 gives the beam power absorbed by the coil in W/g .

If we assume as a first-order approximation that the whole beam energy of SLAC (20×10^9 eV) is concentrated in a beam with the radius $r = 0.3$ cm and an average current of 25×10^{-6} A passes through the magnet, we get from Eq. (8):

$$-\frac{n_m}{n_0} \cdot \frac{dE}{dX} = 1.6 \times 10^8 .$$

For the magnet with an average density of $\delta = 5$ g/cm³, one obtains

$$X_0 = 15 \text{ g/cm}^2 .$$

The beam current density is

$$J_b = 1.06 \times 10^{-4} \text{ A/cm}^2 ,$$

and thus the power absorbed in the magnet:

$$p_a = -\frac{n_m}{n_0} \cdot \frac{dE}{dX} \cdot J_b = 1.6 \times 10^8 \times 1.06 \times 10^{-4} \cong 1.7 \times 10^4 \frac{W}{g} .$$

The calculation of power density for a point beam gives excessive values. In fact, the high-energy beam has a finite cross section and the above calculation must be modified for more realistic cases. The power density for a diffuse source is calculated by Guiragossian¹¹ using Monte Carlo computation. The result of his calculation for a thick copper target is illustrated in Fig. 5. The radial extension of shower is estimated from 2π revolution of the Gaussian beam distribution. The incident beam power of 1 MW/cm is modified in Curves 2 and 3 to determine the power density in

11. Z. Guiragossian, Technical Note SLAC-TN-63-85 (1963).

W/g in Curve 3. The beam radius at $L = 0$ is 0.52 cm.¹¹ For the incident beam power of 1 MW, the power density at shower maximum is 9.3×10^3 W/g.

If the beam is missteered and may hit the coil for only one second before the interlock may interrupt the beam, the energy of 9.3×10^3 J/g is absorbed by the coil at shower maximum, corresponding to 9.3×10^8 rad. In this case, the coil heating is more intensive than the ionization effect due to irradiation. If the magnet is protected by means of collimators and only a fraction collides with the coil, Curve 3 in Fig. 5 can be modified accordingly in order to determine the absorbed beam power at shower maximum.

4. Expected Average Radiation Dose in Magnet Coils

In order to calculate the expected long-term integrated radiation dose in a magnet coil, we assume that a magnet is located 5 m from a collimator and a beam power of 10 kW is passed to the coil. This part will be partly scattered, partly absorbed.

The intensity of the scattered part of the beam decreases with the deflection angle according to:

$$\frac{1}{I_0} \frac{dI}{d\Omega} = \begin{cases} \frac{1}{\pi (\theta^2)_{av}} & \text{for } \theta^2 < (\theta^2)_{av} \\ \frac{(\theta^2)_{av}}{\pi \theta^4} & \text{for } \theta^2 > (\theta^2)_{av} \end{cases}$$

We assume the radial distance of the coil is 5 cm from the beam axis; thus:

$$\theta = 10^{-2}$$

Using mean square angle of deflection, we write according to Rossi¹⁰

$$(\theta^2)_{av} = \left(\frac{E_s}{E_0} \right)^2 \cdot \frac{X}{X_0} \quad (9)$$

with

$$\begin{aligned} E_s &= \left(\frac{4\pi}{\alpha} \right)^{\frac{1}{2}} \cdot m_e c^2 \\ &= 21 \text{ MeV} . \end{aligned} \quad (10)$$

For the particular case of SLAC with $E_0 = 20 \times 10^9$ eV, we get:

$$(\theta)_{av} = 1.05 \times 10^{-3} \left(\frac{X}{X_0} \right) .$$

For $X = X_0$, we have

$$(\theta^2)_{av} = 1.1 \times 10^{-6} < \theta^2 = 10^{-4}$$

and thus:

$$\frac{1}{I_0} \frac{dI}{d\Omega} = \frac{(\theta^2)_{av}}{\pi \theta^4} = \frac{1.1 \times 10^{-6}}{\pi \times 10^{-8}} = 3.5 \times 10^1 \text{ sr}^{-1} .$$

At 5 m distance, the current density of the scattered beam is:

$$J_{sc} = 3.5 \times 10^1 / 2.5 \times 10^5 = 1.4 \times 10^{-4} I_0 \text{ (A/cm}^2\text{)}$$

$$\equiv I_0 / A_{eff} ,$$

which corresponds to an effective area of $A_{eff} = 7.2 \times 10^3 \text{ cm}^2$. For 10 kW beam power passed unaffected to the magnet, we get from Fig. 5

$$\frac{\partial P}{\partial W} = \frac{1}{\gamma A_X} \cdot \frac{\partial P}{\partial X} = 97 \text{ W/g}$$

at shower maximum, and

$$\frac{\partial P}{\partial W} = 11 \text{ W/g} \quad \text{at } X = X_0 .$$

The power density at the magnet is decreased, because the effective beam area is increased, i.e.,

$$\left(\frac{\partial P}{\partial W} \right)_{coil} = \left(\frac{\partial P}{\partial W} \right)_{X=X_0} \cdot \frac{A_{X_0}}{A_{eff}} = 11 \cdot \frac{0.87}{7.2 \times 10^3} = 13.3 \times 10^{-4} \text{ W/g} .$$

The power density per unit volume is:

$$P_v = \delta \cdot \left(\frac{\partial P}{\partial W} \right)_{coil} = 5 \times 13.3 \times 10^{-4} = 6.65 \times 10^{-3} \text{ W/cm}^3 .$$

The total dose rate is given by the simple relation:

$$D = \left(\frac{\partial P}{\partial W} \right)_{coil} \cdot t \cdot 10^7 \text{ (erg/g)}$$

with t in seconds.

III. RADIATION EFFECTS ON TYPE II SUPERCONDUCTORS

When materials are irradiated, their properties are changed in a variety of ways, which are briefly summarized:

- a) Disordering effect of irradiation alters lattice irregularity (thermal and electrical conductivity).
- b) Mechanical properties are changed (hardness, elongation, ductility).
- c) Atomic displacements and associated phenomena.
- d) Ionization effects.

Production of defects is basically a cascade process, in which the incident irradiation interacts and displaces an atom with sufficient energy. This atom can initiate secondary, tertiary displacements, etc.

Once an atom has received enough energy to dislodge it from its equilibrium lattice site, it moves through the lattice losing its energy through further collisions with other atoms and individual electrons. If the atom is sufficiently energetic, it will be ionized and initially lose energy by ionizing collisions, occasionally displacing other atoms by coulomb scattering collisions.

However, the interactions produce a greater number of recoils. Displacement cross sections for fission neutrons are about 10^{-21} cm². Charged particles (protons, neutrons and alphas) are light and sufficiently energetic (~ 50 MeV). Their energy loss mechanism is primarily ionization (Rutherford scattering). Deuteron cross sections are about $(3-4) \times 10^{-21}$ cm².

Irradiation has at least four effects:

- 1) Exchange of atoms between sites.
- 2) Creation of interstitial vacancy pairs.
- 3) Clustering of vacancies.
- 4) Creation of new elements.

Of the four, the disorder caused by exchange of atoms is most important..

The proposed use of superconducting devices in a radiation environment has been accompanied by studies to determine the extent of radiation effects on such devices. Past and present experiments conducted have shed some light on the current-carrying capacity mechanism of superconducting type II materials. The important property here is creation of defect structures by cold working and irradiation. The importance of defect structures is particularly pertinent in ductile alloys such as NbZr and NbTi. It is recognized that gross radiation effects are similar to the effect of cold work. Both effects yield increase in hardness and tensile strength (indicating embrittlement). Both effects are annealed at approximately the same temperature.

Another important aspect concerns the thermal stability of radiation-induced defects. Many radiation effects anneal out at room temperature (some even at 10⁰K). Most promising experiments are those at liquid helium temperatures.

Information regarding irradiation effects on three widely used, commercially available superconducting type II materials is scattered in the literature. Details of measuring techniques, etc., are not presented here. We give quantitative data for a few of these materials, measured at temperatures below transition temperature.

a) Nb₃Sn

Deuteron irradiation¹ doses up to 10^{17} d/cm² reveal (Fig. 6) that at 5.7⁰K, the critical current density is increased for fields higher than 1 T and is not affected by annealing. At 10.9⁰K, J_c is reduced at all fields and tends toward annealed values. The increased current-carrying capacity is characterized by the Kim-Anderson model

$$J_c = \frac{\alpha}{H + B_0}$$

in the range of 1.... 4.5) T. Large departure from the model is observed at transverse fields higher than 4.5 T, where the H_{c2} values were changed. It was shown that the H_{c2} is of primary, the J_c of secondary importance.

Proton irradiation¹² shows an enhancement of the critical current density

$$\frac{\Delta J}{J_{c0}} = \frac{J_c^{\text{irr}} - J_{c0}}{J_{c0}}$$

in Fig. 7. The enhancement of J_c is independent at first approximation of external field H_a up to 5 T. The irradiated sample does not follow the Kim-Anderson model, although nonirradiated samples do. Similarity to heavily cold-worked Nb_3Zr alloys is evident at medium fields, where J_c is independent of H_a . The maximum value of $\Delta J/J_{c0}$ is measured at a dose rate of $N_p \cong 8 \times 10^{16}$ p/cm². At higher irradiation doses, ΔJ decreases.

Neutron irradiation.¹³ The critical current J_c and demagnetization factor α of Nb_3Sn tubes placed in a reactor were enhanced up to 50%, after irradiation with a dose rate of 2×10^{18} fast neutrons/cm². The magnetic field at the specimen was ~ 2 T. The increase in α (Anderson's model) and J_c are responsible, however, for a more unstable performance by exhibiting more flux jumping than the nonirradiated sample. Power dissipation (due to flux creep) increases exponentially with α and leads to instabilities. Neutrons produce defect clusters with fluxoid pinning energies comparable to those already present in Nb_3Sn due to cold work. Measurements¹⁴ at low fields (~ 0.4 T) indicate for diffusion-processed Nb_3Sn an enhancement in J_c by a factor of 2.7, while the critical temperature was decreased by 0.08°K . The radiation dose was 10^{18} n/cm² and the preradiation current density 10^5 A/cm². Unfortunately no neutron irradiation data at fields higher than 2 T are available at present.

b) Nb_3Zr Alloys

Deuteron irradiation.¹ Copper-coated samples irradiated show a post-irradiation depression of the critical temperature of $0.2 \dots 0.8^\circ\text{K}$. Samples not copper coated show little or no change in T_c ($< 0.2^\circ\text{K}$). No great changes were observed in the critical current density except in the region near the upper critical field. Recovery at annealing was observed as in Nb_3Sn alloys. Measurements had been performed up to 10^{17} (15 MeV) d/cm² (Fig. 8).

Neutron irradiation. Irradiation with fast neutrons up to 10^{18} n/cm² did not reveal significant changes up to fields of 2 T. It is believed that near the upper critical field, the current density will again exhibit peak effects, as observed in the case of deuteron irradiation.

Proton irradiation. No detailed experiments have been reported.

c) $\text{Nb61}\% \text{Ti}$ Alloys

Deuteron irradiation.¹ As seen from Fig. 9, critical current density is reduced, specifically at fields between 4 and 5 T, indicating also a reduction of the upper critical field. Post-curing to 77°K restores

12. H.J. Bode and K. Wohlleben, Phys. Letters 24A, 25 (1967).

13. P.S. Swartz et al., Appl. Phys. Letters 4, 71 (1964).

14. J.P. McEvory, Jr. et al., Appl. Phys. Letters 4, 43 (1964).

preirradiation properties. As no irradiation data above 5 T external fields are measured, it is not clear if peak effects observed for Nb25%Zr are repeated for NbTi.

Neutron and proton irradiation. No data are available at present.

IV. IRRADIATION EFFECT ON NONSUPERCONDUCTING METALS

Copper, aluminum, a few copper alloys, and silver are the few metals which are used extensively in conjunction with superconducting magnets. Irradiation properties of copper have been studied in detail and we report only properties pertinent to the stability of supermagnets.

1. Mechanical Properties

Yield and tensile strengths of electric grade OFHC copper are given in Fig. 10, when subject to various dose rates of fast neutron irradiation. Both yield and tensile strengths are increased, indicating embrittlement. Examination by means of electron microscopes indicates that the high yield stress is caused by kinking of glide dislocations and the low rate of strain hardening is related to blocking free glide planes.

Bombardment by means of neutrons and electrons shows that irradiation causes a strengthening of copper. The decrease in internal friction is a result of pinning dislocations by irradiation. It was even suggested (decrease in internal friction is similar after neutron or gamma irradiation to a temperature quenching) that pinning sites are vacancies. After irradiation, many more defects could be observed, i.e., copper irradiated up to 6.7×10^{17} n/cm² at 35°C contains 3×10^{15} defects per cm³ in the form of small strained regions. After increasing the radiation dose three orders of magnitude to 14×10^{20} n/cm², many more defects, such as dislocation loops, were observed. The defect sizes were increased from 75 Å to about 150 Å. The loops grow by migration of vacancies or vacancy clusters.

2. Electrical Resistivity

The atom-displacement type of damage in copper resulting from fast neutron irradiation causes lattice imperfections. This creates a residual disorder, specifically if irradiation temperature is low compared to the recovery temperature of the metal.

OFHC copper, irradiated at 78°C, shows an increase in resistivity of about 24%, electric grade Al even to 36%, when irradiated up to 10^{19} nvt (integrated neutrons/cm²). High-purity copper, annealed at 90°C, shows an increase in resistivity of only 8%, when irradiated up to 7×10^{20} nvt.

Cooper et al.¹⁵ measured a nearly linear change in resistivity of copper and silver with the number of deuterons bombarding the material at 10°C (10 MeV neutron irradiation). Further investigation shows that lower irradiation temperatures were necessary to immobilize defects produced. A portion of the change in physical properties is annealed and removed during continued irradiation at a given temperature. Room temperature radiation produces little permanent change because the effect of radiation anneals out at radiation temperature. Copper irradiated at 4°C shows some annealing already at 7°C. Nonlinear change in resistivity as a function of radiation dose is

15. H.G. Cooper et al., Phys. Rev. 97, 599 (1955).

attributed to annealing effects. The rate of increase in resistivity during neutron bombardment at 20°C is measured to be 3.1×10^{-11} for copper, 7.9×10^{-11} for aluminum, when bombarded with a neutron flux of 7×10^{11} n/cm²/sec. If annealing of induced defects is prevented, the increase in resistivity is assumed proportional to the number of defects produced in the metal. Annealing at elevated temperatures after irradiation reduces the resistivity to some proportion of the original preirradiation value. The damaging rate at 4.2°K in cold-worked copper is by far greater than for annealed copper.

The effect of neutron irradiation in low-alloy steels has been investigated by Porter.¹⁶ Yield and tensile strengths are increased in the range of 5×10^{18} to 10^{20} n/cm², considered to be about 7×10^3 kg/cm². Up to 10^{15} n/cm², no changes could be measured (Fig. 11). Some measurements indicate that the rate of change in yield and ultimate tensile strengths decreases slightly after exposure of 2×10^{21} n/cm².

The irradiation-induced hardening occurs to a greater extent in fully annealed materials than in steels purposely hardened prior to irradiation, or at cryogenic temperatures.

Magnetization properties of low-alloy steels have not been investigated as a function of irradiation dose.

V. IRRADIATION EFFECTS ON INSULATIONS

Insulations in superconducting magnets are generally based on polyamides (Nomex, Nylon), polyethylenes (Mylar), polytetra fluoroethylene (Teflon), phenolic materials, epoxies, silicones, or glass filament epoxy complexes. Due to the cryogenic environment and the high electromagnetic stresses ($> 10^4$ kg/cm², compressive stress; $> 2 \times 10^3$ kg/cm², shear stress), requirements on mechanical and physical properties, specifically fatigue, and thermal expansion are enhanced.

The dielectric stress on the insulations is roughly the same as in water-cooled dc electromagnets, but in order to dissipate the electromagnetic field energy within a few seconds, into external water-cooled resistors, in order to prevent coils from damage after a quench and to preserve helium, voltages in excess of 5 kV may be necessary across the coil terminals. The transient voltage waveform produces voltage gradients between turns in the order of magnitude of several kV/cm. Internally, a few insulation breakdowns, leading to interturn short circuits or layer shorts, have several disconcerting effects:

- a) Current charging time is delayed.
- b) Occurrence of instabilities due to sudden changes of the coil inductance, indicating magnetic field rearrangement over the coil.
- c) Localized increase in ac resistivity in superconductors, producing local regions of normality.
- d) Increase of helium boil-off due to flux motion.
- e) Short circuits between turns and layers become more pronounced and extend over wider areas.
- f) Increased risk that a localized short circuit absorbs the magnet energy in case of a quench. This may produce melting and discontinuity of the conductor. The arc produced internally may destroy the coil.

16. L.F. Porter, Am. Soc. Testing Mater., Spec. Tech. Publ. No. 276.

Radiation properties of most organic insulations have been tested at room or elevated temperatures. Irradiation data at cryogenic temperatures specifically below 21°K are scarce. In the following, it is tried to correlate the existing data to mechanical and electrical properties expected at cryogenic temperatures. Irradiation effects on insulations can be summarized briefly as follows¹⁷:

- 1) Permanent changes. In appearance, color effects ($< 10^5$ rad threshold damage).
- 2) Chemical changes. Double bond formation, cross linking, oxidative degradation, polymerization, depolymerization, gas evolution ($10^6 - 5 \times 10^9$ rad).
- 3) Mechanical changes. Embrittlement, hardness, elongation, tensile and flexural stress, elastic modulus, flexibility ($10^4 \dots 10^{12}$ rad).
- 4) Physical changes. Thermal conductivity, dielectric constant, volume resistivity, dissipation factor, heat distortion ($10^5 \dots 10^{13}$ rad).

Several reactions may occur simultaneously. The initial effect is a curing process which improves tensile, flexural and shear stress by cross linking. The percentage elongation is reduced. The end result is always a structure highly cross-linked, fragile, and crush-sensitive.

At cryogenic environments, the irradiation effects are marked by low temperature effects. Tensile and elongation properties are enhanced considerably at low temperatures. The degradation of mechanical properties due to irradiation is again considerable, as in air at room or elevated temperatures, but they are vastly improved, compared to air radiation values. From the few available data¹⁸ it is difficult to predict systematic changes of insulation materials, and thus materials are discussed in groups:

1) Teflon TFE and FEP (films)

Material thickness and manufacturing procedure are probably the most important parameters in evaluation of irradiation properties. Thin films (5×10^{-3} to 10^{-2} cm) are more radiation resistant than thick films (0.1 cm thick). However, the data obtained are not systematic and the trend not predictable. Thickness and environmental effects reduce the ultimate elongation by a factor of 2 to 3.

Results obtained for 0.025 cm thick TFE film are summarized in Tables IA and IB.

At room temperature, evaluated elongation values for various thicknesses of Teflon FEP (Fluorinated Copolymer of Ethylene and Propylene) show one order of magnitude improvement in radiation dose, compared to Teflon TFE.

17. H. Brechna, Report SLAC 40 (1965).

18. E.E. Kerlin and E.T. Smith, General Dynamics, Fort Worth, Texas, Reports FZK 188-1 (1964), FZK 188-2 (1964), and FZK 290 (1966).

TABLE IA

Mechanical Properties of Teflon TFE (0.025 and 0.3 cm thick)

Average Temperature (°K)	Average Pressure (mm Hg)	γ Irradiation Dose (rad)	Ultimate Tensile Strength (kg/cm ²)	Ultimate Elongation (%)
300 ^a	760	0	282 ± 70	270 ± 50
300 ^a	~ 10 ⁻⁶	9 × 10 ⁵	191 ± 14	180 ± 10
300 ^a	10 ⁻⁶	5 × 10 ⁷	91.7 ± 5	99 ± 3
78 ^b	760	0	705.0	5.2
78 ^b	760	10 ⁷	564	2.15
21 ^b	760	0	820	3.2
21 ^b	760	7.5 × 10 ⁶	800	2.45
21 ^b	760	4 × 10 ⁹	785	1.95

a) 0.025 cm thick

b) 0.3 cm thick

TABLE IB

Electrical Properties of Teflon TFE (0.3 cm thick)

Average Temperature (°K)	Average Pressure (mm Hg)	γ Irradiation Dose (rad)	Dielectric Constant ^a	Dissipation Factor	Volume Resistivity (Ω·cm)
297	760	0	1	<2 × 10 ⁻⁴	>5 × 10 ¹⁷
89	5 × 10 ⁻⁷	0	1.015	<2 × 10 ⁻⁴	>5 × 10 ¹⁷
297	760	9.5 × 10 ⁷	0.9977	4.5 × 10 ⁻³	2 × 10 ¹⁴
88	3 × 10 ⁻⁷	9.5 × 10 ⁷	1.019	2.6 × 10 ⁻³	>5 × 10 ¹⁷

a) In the table, normalized dielectric constant is used to compare data. The true dielectric constant at room temperature and atmospheric pressure is 2.0.

2) Kynar 400* (Halocarbon)

Fluorocarbon plastics, such as Kel F and some Teflons, are widely used in superconducting magnet systems. As seen, Teflon has poor radiation properties in air. The irradiation properties improve, however, if radiation and tests are performed in vacuum and at cryogenic temperatures. Kynar, used frequently in aerospace applications, may be useful for conductor insulations; it is a thermoplastic resin containing 59% Fluorine. It has improved irradiation stability, as seen from data for film specimens given in Tables IIA and IIB:

* Trade name. Pensalt Chemical Corporation.

TABLE IIA

Electrical Properties of Kynar 400

Average Temperature (°K)	Average Pressure (mm Hg)	Gamma Dose (rad)	Dielectric Constant ^a	Dissipation Factor	Volume Resistivity (Ω·cm)
<u>Vacuum-Cryotemperature-Irradiation Tests</u>					
297.5	760	0	1.000	4.2×10^{-3}	4×10^{15}
81.0	2×10^{-6}	0	0.5756	1.4×10^{-3}	$>6 \times 10^{15}$
80.0	2×10^{-6}	6.6×10^7	0.5845	7.5×10^{-3}	$>6 \times 10^{15}$
116.0	2×10^{-6}	1.7×10^7	0.6154 ^b	2.51×10^{-2b}	1×10^{14}
286	760	6.6×10^7	0.9880	1×10^{-2}	5×10^{13}
<u>Air-Irradiation Tests</u>					
286	760	0	1.000	3.8×10^{-3}	8×10^{14}
291	760	2.1×10^8	0.9994	5.6×10^{-3}	1×10^{10}

a) Normalized. Actual value at 300°K and 1 atm pressure is 4.

b) Values obtained during irradiation at highest dose rate.

TABLE IIB

Mechanical Properties of Kynar 400

Average Temperature (°K)	Average Pressure (mm Hg)	Radiation Exposure		At Rupture	
		Gamma Dose (rad)	Neutrons E>2.9 MeV (n/cm ²)	Tensile Strength (kg/cm ²)	Elongation (%)
297	760	0	0	325	91
333 ^a	760	9.7×10^7	2×10^{15}	520	7
366	760	1.7×10^9	2.5×10^{16}	354	4.2
333 ^b	2×10^{-6}	8.5×10^7	1.7×10^{15}	565	19.2
333 ^c	2×10^{-6}	9.2×10^7	1.5×10^{15}	290	6.2
77 ^d	760	0	0	1460	1.75
77 ^e	760	7.8×10^7	1.4×10^{15}	920	1.42
21 ^f	760	0	0	1425	2.15
21 ^g	760	7.9×10^7	1.4×10^{15}	940	1.44

a) Tested in air, measured in air.

b) Irradiated in vacuum, tested in air.

c) Irradiated and tested in vacuum.

d) Tested in liquid nitrogen.

e) Irradiated and tested in liquid nitrogen.

f) Tested in liquid hydrogen.

g) Irradiated and tested in liquid hydrogen.

3) Kepton (H-Film)

Kepton is a polyamid film and has a unique blend of physical, electrical and mechanical properties. Its dielectric constant is invariable in the range of 298°K to 473°K. It shows excellent irradiation properties up to 8.8×10^7 rad; its contraction coefficient is best compatible to stainless steel and thus it is used frequently as a barrier in glass filament-epoxy structures against diffusion of gases and cryogenic liquids. It is used only in limited applications in superconducting magnets. Specimens of 5×10^{-3} cm thick films tested in air at room temperature, exhibit a change in tensile strength and break at 3.3×10^8 rad, and a noticeable damage at 1.7×10^9 rad. The initial value of elongation (109%) changed to 66% at 3.3×10^8 rad, and to 98% at 1.7×10^9 rad. There were no apparent color changes during test.

Presently, no data on irradiation properties of H-Films at cryogenic temperatures are available.

4) Lexan*

Lexan is a polycarbonate plastic and is used in some high-energy superconducting magnets. Its room temperature properties are excellent. At 10^8 rad, Lexan changes color and becomes dark; however, it retains its transparency. Threshold value for embrittlement is 10^8 rad. At 10^9 rad, gamma irradiation caused swelling, severe embrittlement, and general disintegration.

Electrical properties of Lexan are given in Table IIIA. Room temperature mechanical properties are presented in Table IIIB. No mechanical tests at cryogenic temperature vs irradiation dose are reported.

TABLE IIIA
Electrical Properties of Lexan

Average Temperature (°K)	Average Pressure (mm Hg)	γ Irradiation Dose (rad)	Dielectric Constant ^a	Dissipation Factor	Volume Resistivity (Ω·cm)
297	760	0	1	1.2×10^{-3}	6×10^{15}
286	760	6.6×10^7	0.982	1.4×10^{-3}	7×10^{14}
77	2×10^{-6}	6.6×10^7	0.9612	1.9×10^{-3}	5×10^{17}
<u>Tests in air</u>					
286	760	0	1	1.5×10^{-3}	2×10^{15}
290	760	2.1×10^8	0.997	1.9×10^{-3}	3×10^{12}

a) The values given in Table IIIA are normalized. The true dielectric constant of Lexan at room temperature and atmospheric pressure is 3.0.

*Trade name. General Electric Company.

TABLE IIIB

Room Temperature Mechanical Properties of Lexan

Average Temperature (°K)	Average Pressure (mm Hg)	Radiation Exposure		Ultimate Tensile Strength (kg/cm ²)	Ultimate Elongation (%)
		Gammas (rad)	Neutrons E>2.9 MeV (n/cm ²)		
297	760	0	0	685	5
333 ^a	760	9.7×10^7	2×10^{15}	250	1.7
364 ^a	760	1.7×10^9	2.5×10^{16}	too brittle to test	
333	2×10^{-6}	8.5×10^7	1.7×10^{15}	466	8

a) Irradiated in air, tested in air.

b) Irradiated under vacuum, tested in air.

5) Mylar

Mylar, a polyethylene terephthalate, is quite commonly used in superconducting magnets for interturn and interlayer insulation. As seen from Table IV, at a dose of 5.7×10^6 rad, mechanical properties are improved. Degradation starts before 9.7×10^7 rad and at 1.6×10^9 rad, the samples were too brittle to permit testing. Vacuum-irradiated samples behaved similarly. No data at cryogenic temperatures are available.

TABLE IV

Room Temperature Mechanical Properties of Mylar

Average Temperature (°K)	Average Pressure (mm Hg)	Radiation Exposure		Rupture Tensile Strength (kg/cm ²)	Rupture Elongation (%)
		Gammas (rad)	> 2.9 MeV Neutrons (n/cm ²)		
297 ^a	760	0	0	1700	80
297 ^a	760	5.7×10^6	1.4×10^{14}	1700	91
311 ^a	760	5.2×10^7	1.1×10^{15}	1610	100
333 ^a	760	9.7×10^7	2×10^{15}	1280	65
350 ^a	760	3.3×10^8	5.4×10^{15}	too brittle to test	
300 ^b	5×10^{-7}	2.4×10^6	4.4×10^{13}	1750	89
311 ^b	2×10^{-6}	8.5×10^7	1.7×10^{15}	1370	87
300 ^c	5×10^{-7}	2.4×10^6	4.4×10^{13}	1470	167
325 ^c	9×10^{-7}	5.3×10^7	9.7×10^{14}	1100	44

a) Irradiated in air, tested in air.

b) Irradiated under vacuum, tested in air.

c) Irradiated under vacuum, tested in vacuum.

6) Thermoset Laminates

Glass fiber epoxy laminates are widely used as spacers, structural supports, pancake insulation for radial cooling, etc., in cryogenic magnets. Ample data on irradiation properties are available at room temperature¹⁹ but test results at cryogenic temperatures are scarce.

Extensive data for Lamicoid 6038E (melamine-fiberglass) are presented by Kerlin and Smith¹⁸ and Tables VA and VB reflect their measurements. These data are representative for glass fiber epoxy structures as well, and may be used to determine irradiation damage in interlayer and interturn insulations.

TABLE VA

Electrical Properties of Melamine-Fiberglass Lamicoid

Average Temperature (°K)	Average Pressure (mm Hg)	γ Irradiation Dose (rad)	Dielectric Constant ^a	Dissipation Factor	Volume Resistivity (Ω·cm)
<u>Vacuum-Cryotemperature-Irradiation Tests</u>					
297	760	0	1	1.9×10^{-3}	7×10^{14}
86	2×10^{-6}	0	0.86	1.3×10^{-3}	3×10^{15}
287	760	6.6×10^7	0.99	1.7×10^{-3}	1×10^{15}
79	2×10^{-6}	6.6×10^7	0.866	1.8×10^{-3}	$>5 \times 10^{15}$
<u>Air-Irradiation Tests</u>					
286	760	0	1	2.6×10^{-3}	6×10^{14}
340	760	2.1×10^7	1.025	2.8×10^{-3}	2×10^{14}
290	760	2.1×10^7	0.999	3.2×10^{-3}	2×10^{12}

a) Normalized dielectric constant. True value of melamine-fiberglass at room temperature and atmospheric pressure is 6.6.

19. M.H. Van de Voorde and G. Pluym, Report CERN MPS/Int Co., 66-25 and 66-27 (1966).

TABLE VB

Mechanical Properties of Melamine-Fiberglass

Average Temperature (°K)	Average Pressure (mm Hg)	Radiation Exposure		Rupture Tensile Strength (kg/cm ²)	Rupture Elongation (%)
		γ Irradiation (rad)	Neutrons (n/cm ²)		
297	760	0	0	4060	2.18
366 ^a	760	1.7×10^9	2.5×10^{16}	3830	2.09
333 ^b	2×10^{-6}	9.7×10^7	2.0×10^{15}	3520	1.63
333 ^c	2×10^{-6}	9.7×10^7	2.0×10^{15}	4200	4.38
116 ^d	0.2 - 0.02	0	0	9000	7.15
94 ^e	0.13 - 0.07	1.2×10^8	9.4×10^{14}	7680	7.36
21 ^f	760	0	0	8000	8.5
21 ^g	760	6.2×10^7	1.1×10^{15}	8300	7.53
21 ^g	760	2.3×10^8	4.1×10^{15}	7750	7.42

- a) Tested and irradiated in air.
 b) Irradiated in vacuum, tested in air.
 c) Irradiated and tested in vacuum.
 d) Tested at LN₂ temperature.
 e) Irradiated and tested at LN₂ temperature.
 f) Tested at LH₂ temperature.
 g) Irradiated and tested at LH₂ temperature.

As expected, the glass fiber tapes or cloth impregnated with melamines, epoxies or silicones are radiation resistive up to dose rates of 10^{10} rad in air. The radiation resistance is improved considerably at cryogenic temperatures. The radiation dosage for the above tests should be extended to 10^{12} rad at liquid helium temperature (4.2°K) in order to make predictions about the performance of insulations for superconducting magnets.

Chemical Reactions

It is known that irradiation causes formation of H₂ and N₂ gases and produces radioactive isotopes (e.g., tritium). At cryogenic temperatures, no measurements of gas evolution are reported. Presumably gas evolution is reduced at liquid helium temperature. It is hoped that most gases produced, freeze inside the insulation material prior to penetration into liquid helium.

Data on gas evolution at room temperature are given below:

<u>Teflon TFE</u>	0.022 ml/g at 4×10^6 rad	(threshold 10^4 rad)
	9.0 ml/g at 9×10^8 rad	
<u>Mylar (PT)</u>	1.2 ml/g at 3.3×10^8 rad	(threshold 6×10^7 rad)
<u>Phenolic Fabrics</u>	4.7 ml/g at 3.7×10^8 rad	(threshold 10^8 rad)
<u>Polyethylene Films</u>	38 ml/g at 6.4×10^8 rad	(threshold 10^8 rad)
<u>Glass-filament-epoxy structures</u>	Traces up to 10^{10} rad	(threshold 2×10^{10} rad)

VI. IRRADIATION EFFECTS ON HELIUM

Scattered parts of the beam have to traverse the liquid helium bath, or during shower development, fractions of the beam energy are absorbed by helium. The most interesting phenomena are power absorption and hydrogen evolution from photoreactions.

1. Power Absorption

For processes connected with the passage of electrons and photons of high energy through matter, when energy losses are essentially due to bremsstrahlung and photo-production, respectively, the range is expressed in terms of the radiation length X_0 . For helium, $^{20}X_0 = 93.1 \text{ g/cm}^2$; for a typical magnet, $X_0 \approx 15 \text{ g/cm}^2$. The density of saturated liquid helium at 4.2°K is 0.126 g/cm^3 , and for the magnet, we assume an average density of $\delta_m = 5 \text{ g/cm}^3$. One centimeter of helium corresponds to $1.35 \times 10^{-3} X_0$ and 1 cm depth of the magnet to $0.333 X_0$.

When the beam passes first through a relatively thin layer of helium, no shower is developed. We neglect shower buildup when the beam passes through the Dewar walls with $\Delta \ll X_0$, but we can determine shower buildup when the beam passes through structural parts and through the magnet. This shower buildup will add to the integrated irradiation dose generated in helium. The power absorbed in the helium bath with the magnet immersed in it must be calculated for the various sections of the magnet and Dewar system separately. By assuming that the particles traversing through the magnet-and-Dewar system have essentially the same energy as the incident beam, then, according to Fig. 5, about nine times more reactions are expected at shower maximum within the coil as would occur by passing through helium alone.

The average energy loss per particle by collision per unit length (g/cm^2) was obtained from

$$-\frac{dE}{dX} = \frac{\epsilon_0}{X_0} \quad (5)$$

For liquid helium, the critical energy

$$\epsilon_0 \approx 250 \text{ MeV}$$

and thus

$$-\frac{dE}{dX} = 2.7 \text{ MeV/g/cm}^2$$

which corresponds to:

$$\begin{aligned} -\frac{dE}{dX} &= 2.7 \left(\frac{\text{MeV}}{\text{g/cm}^2} \right) \cdot 93.1 \left(\frac{\text{g}}{\text{cm}^2} \right) \cdot \frac{1}{X_0} \\ &= 250 \frac{\text{MeV}}{X_0} \end{aligned}$$

The fraction of energy absorbed in one radiation length depends on the incident beam energy; e.g., for $E_0 = 20 \text{ GeV}$ (SLAC), one gets:

$$-\frac{dE}{dX} = \frac{250}{20} \times 10^{-3} = 1.25 \times 10^{-2} \text{ per radiation length.}$$

20. O.I. Dovzhenko and A.A. Pomanskiĭ, Soviet Phys. JETP 18, 187 (1964).

For one centimeter of helium, corresponding to $1.35 \times 10^{-3} X_0$, the absorbed beam power is:

$$\frac{\Delta P_{\text{abs}}}{\Delta P_{\text{inc}}} = 1.25 \times 10^{-2} \times 1.35 \times 10^{-3} = 1.7 \times 10^{-5} \frac{W_{\text{abs}}}{W_{\text{inc}}} / 1 \text{ cm He} .$$

Inside the magnet, due to shower production, we estimate the absorbed power from Fig. 5:

$$\frac{\Delta P_{\text{abs}}}{\Delta P_{\text{inc}}} = 9 \times 1.7 \times 10^{-5} = 1.53 \times 10^{-4} \frac{W_{\text{abs}}}{W_{\text{inc}}} / 1 \text{ cm He} .$$

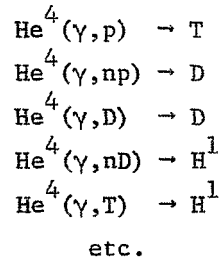
Taking into account shower development in structural parts and thin target type beam absorption in Dewar walls, we estimate a total power absorption of

$$\sim 2 \times 10^{-4} \frac{W_{\text{abs}}}{W_{\text{inc}}}$$

in one centimeter of the depth in the beam direction.

2. Photoreactions

Photoreactions in He^4 lead to various forms of hydrogen, such as H^1 , H^2 , H^3 , etc. The photo disintegration of He^4 can be of the form:



It seems feasible to combine all the reaction products, such as (T, D, H^1 ...) as hydrogen gas. Cross sections for the above reactions are listed up to 150 MeV by Ferguson.²¹ The measurements are made by detecting the number of neutrons released. The number of neutrons are measured from (γ, n) , $(\gamma, 2n)$, as well as (γ, np) and (γ, nD) reactions.

We make the assumption that there is an equality in the following cross sections:

$$\begin{aligned} (\gamma, p) \text{ cross section} &\cong (\gamma, n) \text{ cross section} \\ (\gamma, D) \text{ cross section} &\cong (\gamma, np) \text{ cross section} \\ (\gamma, T) \text{ cross section} &\cong (\gamma, 2n, 2p) \text{ cross section} \end{aligned}$$

Thus measuring neutrons from the (γ, n) , (γ, np) and $(\gamma, 2n, 2p)$ reactions is equivalent to measuring neutrons from (γ, p) , (γ, D) and (γ, T) reactions.

21. G.A. Ferguson et al., Phys. Rev. 95, 776 (1954).

If the reaction cross sections were large, one could approximate

$$\frac{\int \sigma dk}{k^2} \text{ by } \frac{\int \sigma dk}{k_0^2} \quad (k_0 = 25 \text{ MeV}) .$$

Using cross section values obtained by integration of $\int \sigma dk$ by Costa et al.,²² we have, for a photon energy of 50 MeV:

$$50 \text{ MeV} \rightarrow 72 \text{ mb} \cdot \text{MeV}$$

and thus:

$$\frac{\int \sigma dk}{k_0^2} = \frac{72 \text{ mb} \times \text{MeV}}{(25)^2 (\text{MeV})^2} = \frac{110 \text{ } \mu\text{b}}{\text{MeV}}$$

which is a conservative estimate of the D, T, and H yield.

According to DeStaebler,²³ the differential photon track length (Approximation A) from the absorption of an electron with energy E_0 is:

$$\frac{dN}{dk} = 0.57 \frac{E_0}{k^2} X_0 \quad . \quad (11)$$

Accordingly, for the absorption of a beam current I , one may write:

$$\begin{aligned} R &= fI \int 0.57 \left(E_0 \cdot \frac{dk}{k^2} X_0 \right) g \cdot \frac{N_0}{A} \sigma(k) \\ &\cong 0.57 f (IE_0) g \cdot \frac{X_0 N_0}{A} \int_0^{E_0} \frac{\sigma(k)}{k^2} dk \end{aligned} \quad (12)$$

where

IE_0 = total beam power,

fIE_0 = fraction of beam power absorbed,

g = atomic abundance of parent nuclide $\cong 1$,

N_0 = Avogadro number,

A = atomic weight,

$\sigma(k)$ = cross sections.

For 100 kW beam power, we have:

$$IE_0 = 6.25 \times 10^{17} \text{ MeV/sec} .$$

22. S. Costa et al., *Il Nuovo Cimento* 42B, 382 (1966).

23. H. DeStaebler, Technical Note SLAC-TN-62-10 (1962).

In Section VI.1, we calculated for one watt of incident beam power the absorbed power value of 2×10^{-4} W in one centimeter of helium. For 10^5 W of incident beam power, one gets, from Eq. (12):

$$R = 6.25 \times 10^{17} \times 2 \times 10^{-4} \times 1 \times \frac{93.1 \times 6 \times 10^{23}}{4} \cdot 1.1 \times 10^{-28} \text{ atoms/sec}$$
$$= 3.2 \times 10^{10} \text{ atoms/sec}$$

of hydrogen evolved per 100 kW of electron beam power. This is equivalent to 6×10^{-13} liter/sec in one centimeter of helium. These gases may freeze in the coolant passages of the magnet, or contaminate the refrigeration system.

VII. CONCLUSION

Activation due to beam absorbers endangers long-time reliability of magnets more than particle beam missteering, which generates heat, but if the beam current can be interrupted fast enough, the generated heat in magnets can be absorbed.

The effects of nuclear irradiation in various materials are diverse and should be treated separately:

1) Superconducting type II materials

Changes in critical current density are different for various types of superconductors. Nb_3Sn exhibits at low initial J_c a marked enhancement in J_c and α , making the conductor more flux jump sensitive. In NbTi and NbZr alloys, J_c is either reduced or is unchanged, with the exception of peak effect near the H_{c2} region, indicating production of new defects. H_{c2} is generally reduced in all three types of type II superconductors, as well as T_c .

Annealing to room temperature recovers initial conditions to a large extent.

2) Normal metals

At low integrated dose rates $< 10^8$ rad, no major changes in physical properties are encountered. Material embrittlement is primarily due to cryogenic environment rather than induced activity. At higher dose rates, the resistivity of coppers, Al, and Ag is increased markedly. Thermal conductivity is reduced. Ultimate tensile strength is increased and elongation reduced. At very high dose rates, ultimate tensile strength is decreased subsequently.

3) Insulation materials

Irradiation tests on organic insulations (thermoplastic films and thermosetting compounds) are carried down only to liquid hydrogen temperatures. The irradiation effects are generally masked by the cryogenic environment. However, marked improvements against radiation damage are measured in mechanical properties, while electrical properties are less affected. Ionization effects measured during air radiation are reduced. Improvement in irradiation properties is in most insulations one order of magnitude, in some others even two orders of magnitude, compared to room temperature values. Gas evolution is markedly reduced. It is believed that generated isotopes freeze within the insulation matrix and may cause internal damage to the matrix structure before penetrating into the coolant.

The most dangerous effect is production of internal short circuits inside the coil between turns and layers which increase the current charging time constant, produce additional ac losses, or, in case of quenches, may lead to a melting of the conductor and destruction of the coil due to energy dissipation in the short circuit area. No safety precautions can be foreseen for internal failures.

4) Helium

Helium evaporation is enhanced, but is in most cases less alarming. Production of isotopes, even in small quantities, inside the coil body in coolant passages is of concern, which in frozen condition may impare cooling or contaminate the refrigeration system.

Generally speaking, there is a considerable lack of irradiation data at liquid helium temperature. Specifically, a broad-range testing program is needed to determine the performance of insulation materials and normal shunt materials at liquid helium temperature. Tests on type II superconductors are required up to high fields, even, if possible, up to H_{c2} values, to correlate observations reported in the literature and in this paper. Evaluation of fatigue properties of insulations and superconductors is required.

Prior to any wide-range applications of superconducting magnets for beam transport and accelerators, it is imperative that test magnets should be placed and operated in high-irradiation environments in order to predict long-time coil performance.

ACKNOWLEDGMENT

Mr. T.M. Jenkins (SLAC) has been most helpful in compiling data, discussing many aspects of irradiation damage, and providing necessary information for induced activity. It is a pleasure to acknowledge his assistance.

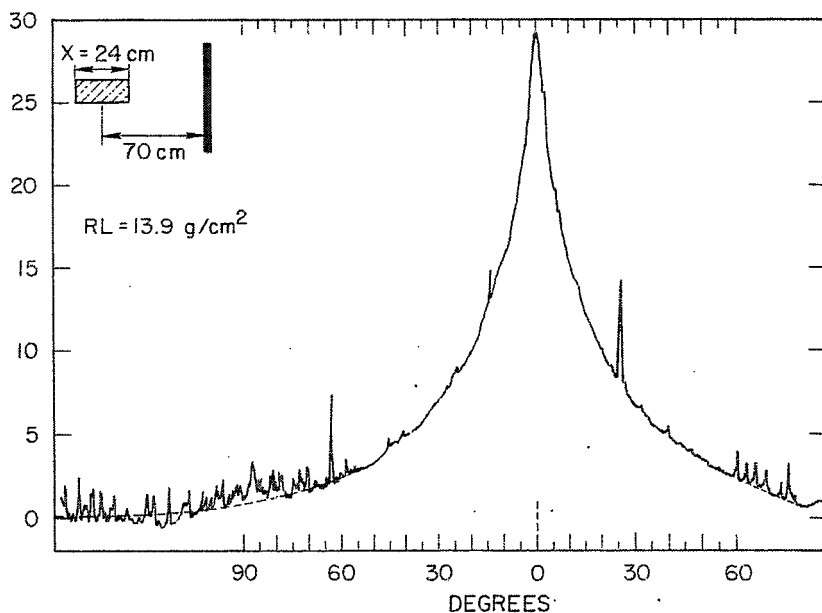


Fig. 1. Angular distribution of gamma dose rate from a typical beam absorber.

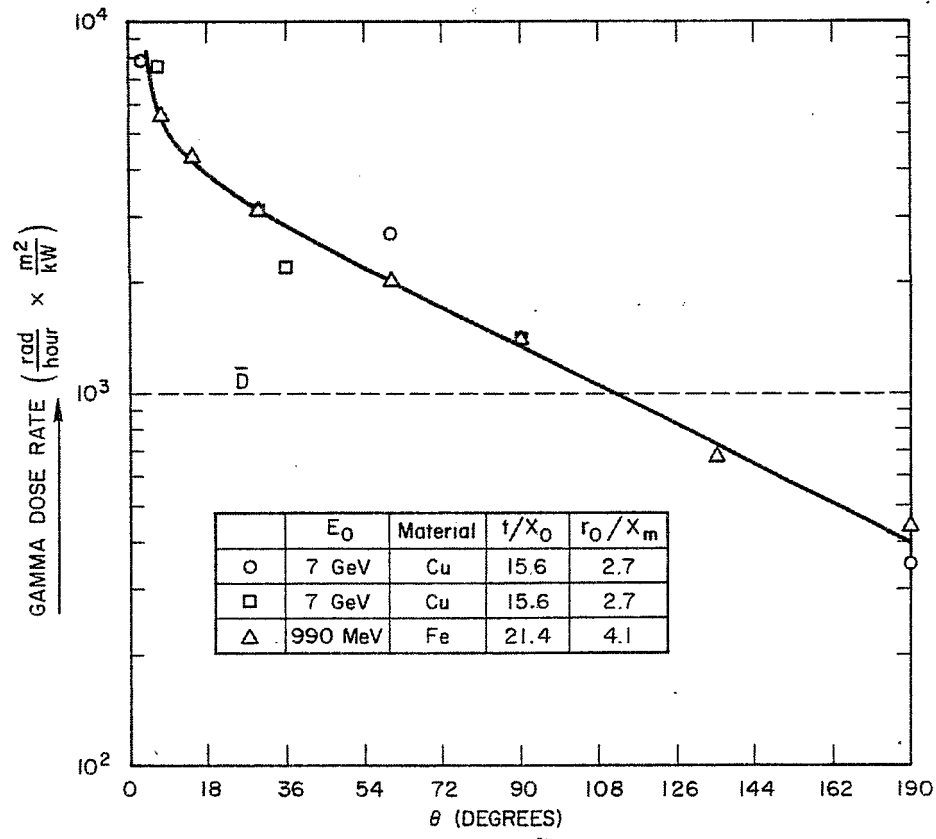


Fig. 2. Gamma dose rate from typical beam absorbers as a function of the angle from the incident beam direction, normalized to 1 kW of beam power and to a source to detector distance of 1 m.

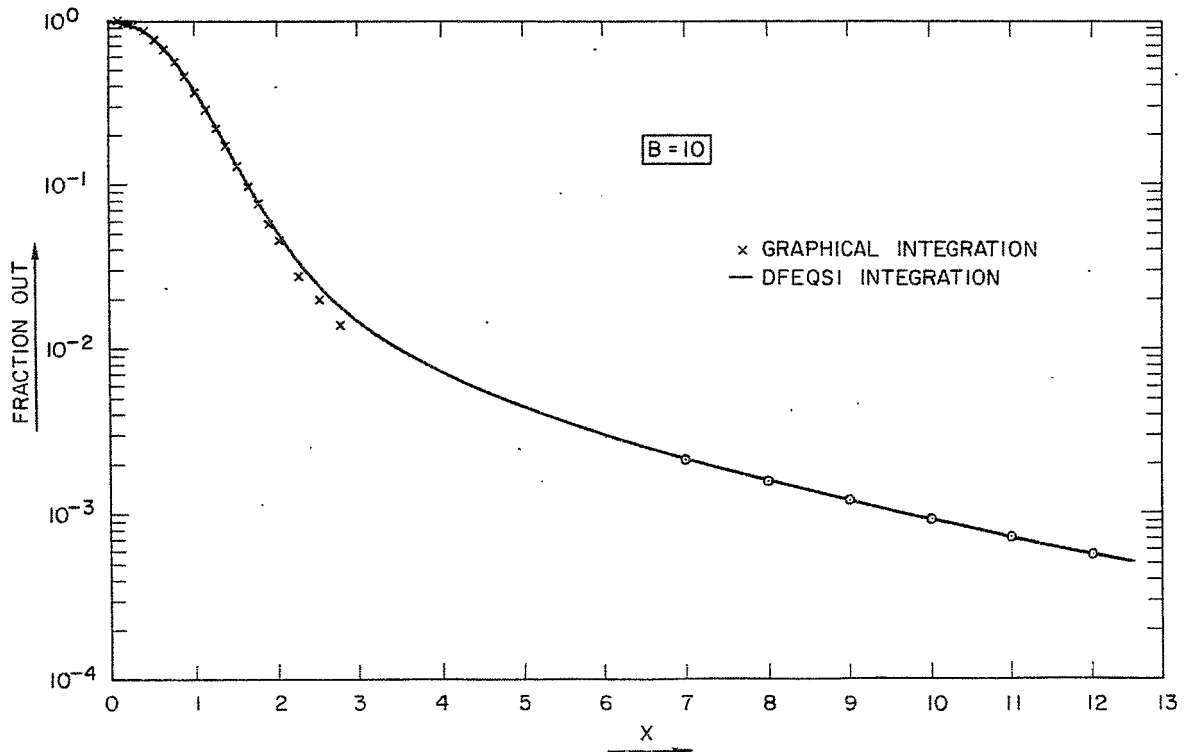


Fig. 3. The fraction of electrons that escape a cone with a space angle $X = \theta / (X_B \sqrt{B})$ vs X for $B = 10$ (copper).

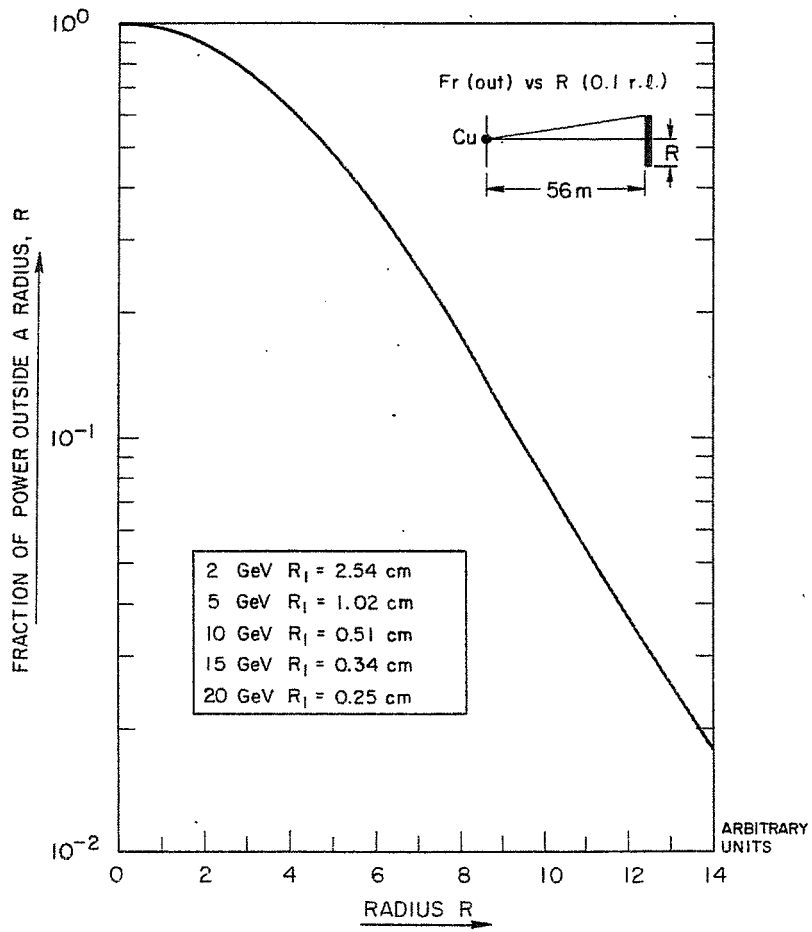


Fig. 4. Fraction of the incident energy that escapes from a thin target.

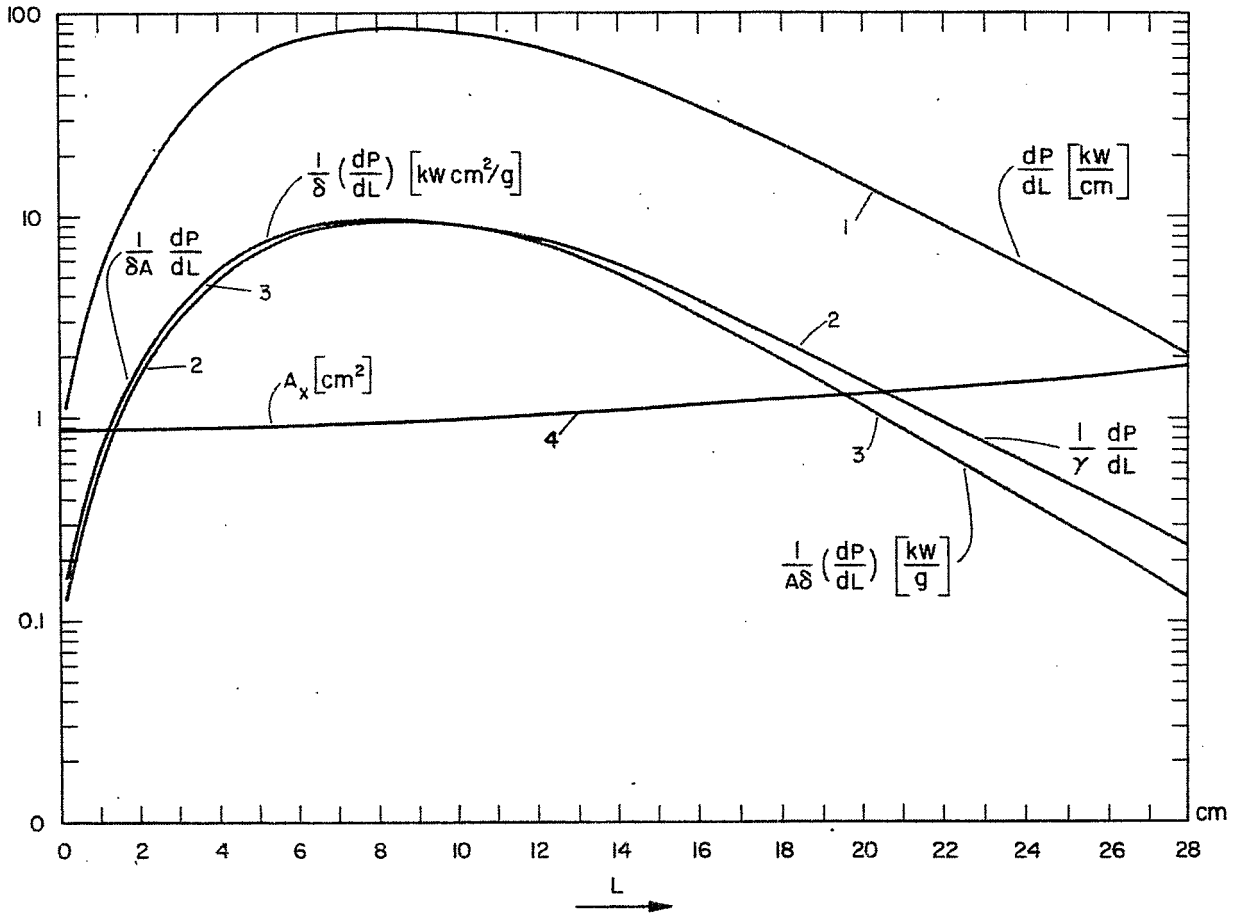


Fig. 5. Longitudinal electron beam power distribution in a shower initiated by electrons of incident energy E_0 in copper.

1. dP/dL (kW/cm) for 1 MW incident beam power.
2. $1/\gamma dP/dL$ (kW cm²/g) for 1 MW incident beam power.
3. $1/\gamma A dP/dL$ (kW/g) for 1 MW incident beam power.
4. Beam cross section A_x in cm².

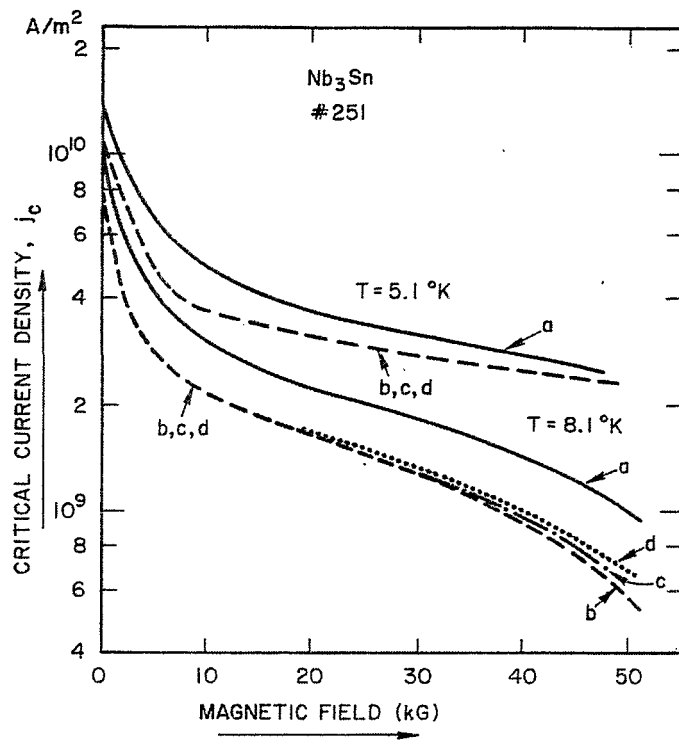


Fig. 6. Critical current density of Nb_3Sn vs applied transverse magnetic field.

- a. Preirradiation.
- b. Irradiated with 10^{17} (15 MeV) d/cm^2 .
- c. Post curing, $77^\circ K$.
- d. Post curing, $300^\circ K$.

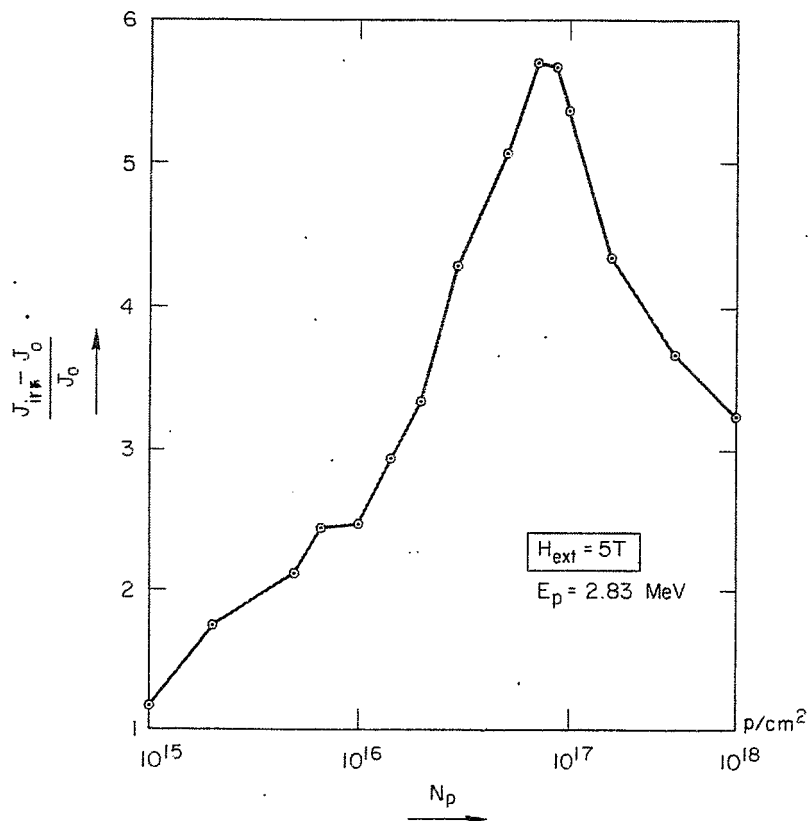


Fig. 7. Enhancement of critical current density for Nb_3Sn diffusion layers as a function of the integrated proton flux N_p/cm^2 . Mean proton energy 2.83 MeV.

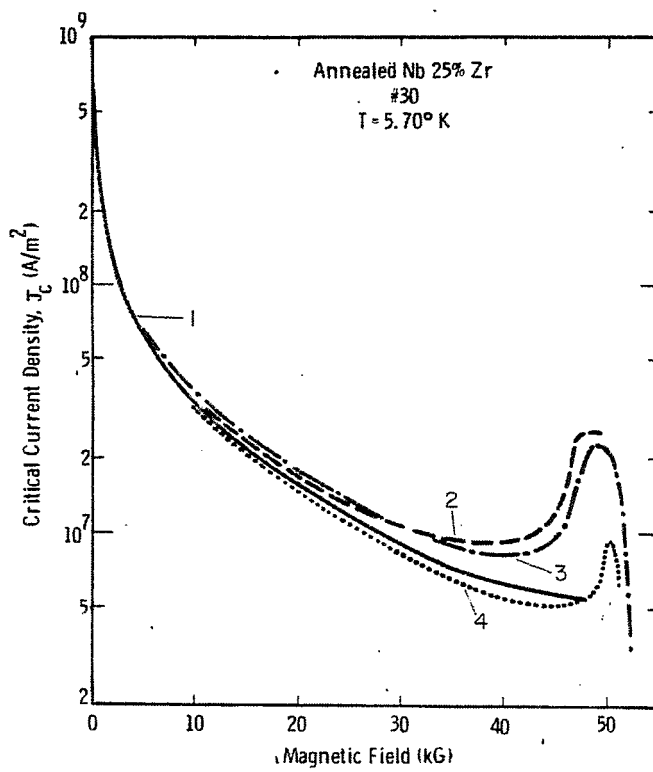


Fig. 8. Critical current density of Nb25%Zr vs applied transverse magnetic field.

1. Preirradiation.
2. Irradiated with 10^{17} (15 MeV) d/cm².
3. Post curing, 77°K.
4. Post curing, 300°K.

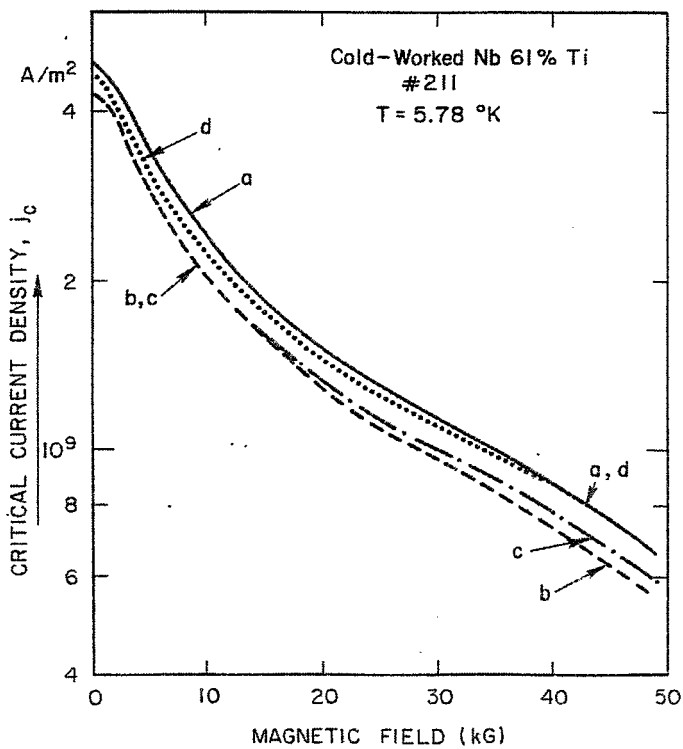


Fig. 9. Critical current density of Nb61%Ti vs applied transverse magnetic field.

- a. Preirradiation.
- b. Irradiated with 10^{17} (15 MeV) d/cm².
- c. Post curing, 77°K.
- d. Post curing, 300°K.

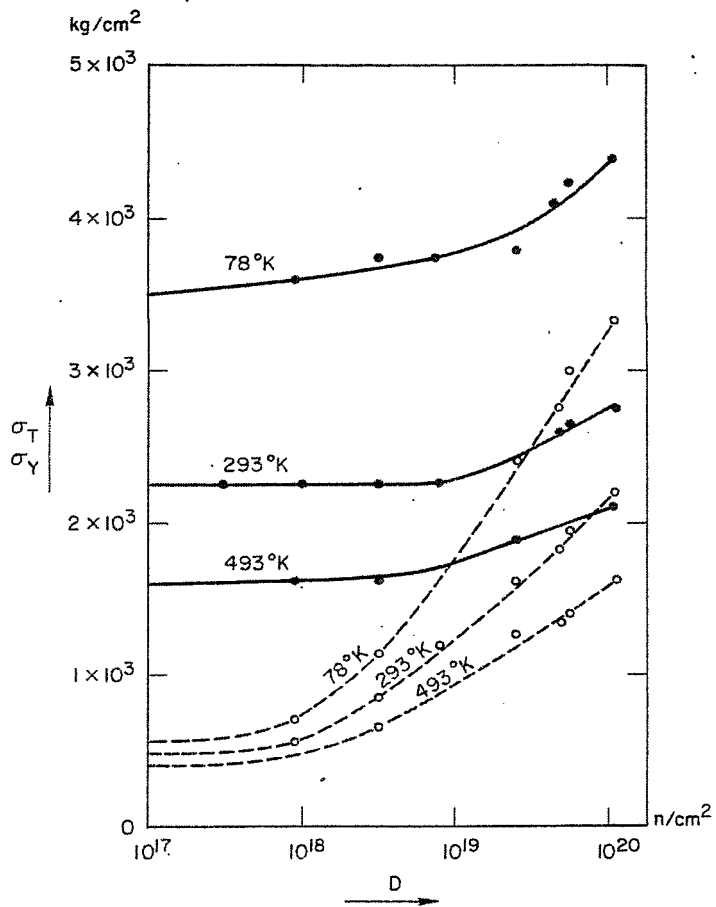


Fig. 10. Ultimate tensile and yield strengths of OFHC copper vs neutron irradiation dose (n/cm^2).

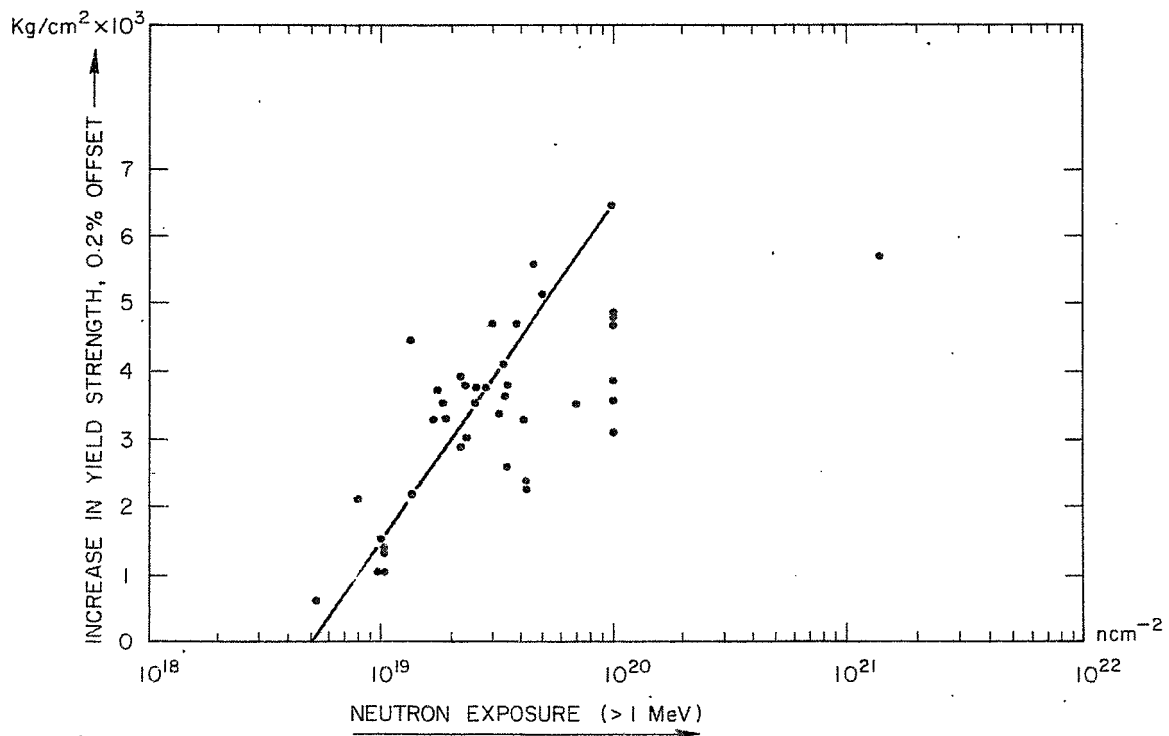


Fig. 11. Effect of neutron irradiation on the yield strength of low-carbon steel (irradiation temperature $< 100^\circ C$).